Journal of Nuclear Materials 390–391 (2009) 259–262

Contents lists available at ScienceDirect

Journal of Nuclear Materials

journal homepage: www.elsevier.com/locate/jnucmat

Impurity seeding and scaling of edge parameters in ITER

H.D. Pacher [a,*], A.S. Kukushkin [b], G.W. Pacher [c], V. Kotov [d], G. Janeschitz [e,1], D. Reiter [d], D.P. Coster [f]

[a] INRS-EMT, 1650 boul. Lionel Boulet, Varennes, QC, Canada J3X 1S2
[b] ITER Organization, Cadarache Centre, F-13108 St. Paul lez Durance, France
[c] Hydro_Québec, 1804, boul. Lionel Boulet, Varennes, QC J3X1S1, Canada
[d] IPP, Forschungszentrum Jülich, D-52425 Jülich, Germany
[e] Forschungszentrum Karlsruhe, P.O. Box 3640, D-76021 Karlsruhe, Germany
[f] Max-Planck-Institut für Plasmaphysik, Boltzmannstr. 2, D-85748 Garching bei München, Germany

ARTICLE INFO

PACS:
52.25.Ya
52.65.Kj
52.65.Pp
28.52.Av

ABSTRACT

ITER divertor and edge modelling with the ITER B2–EIRENE code including neutral–neutral and molecule–ion collisions has led to updated scaling of the helium density and flux and the DT flux with the pumping speed and the divertor neutral pressure. The replacement of carbon by the addition of seeded impurities (neon) strongly modifies the upstream DT density and DT neutral influx at constant detachment state, i.e. divertor neutral pressure and has a smaller influence on the peak divertor power load. The core plasma performance is modelled with the integrated core-pedestal–SOL (ICPS) model implemented in ASTRA; the operating window with seeded impurities is smaller than with DT injection alone.

1. Introduction

B2–EIRENE modelling has been applied extensively to model the ITER divertor with carbon divertor plates. We now use routinely the B2–EIRENE code package version solps4.2 [1–4], which relies on a nonlinear model of neutral particle transport, including neutral–neutral and molecule–ion collisions. The model assumptions are those of [1]. We fix the plasma power entering the scrape-off layer (SOL) at 100 MW, fix the D ion flow from the core across the core-edge interface (CEI) at 17 Pa m^3 s^{-1}, and vary the density with the flux injected by gas puffing. D_2 gas is puffed in, usually from the top, and pumped out via the duct in the private flux region at the bottom of the chamber. The plasma contains ions and atoms of D (representing both D and T), He, and C, as well as D_2 molecules. The present paper extends the previous simulations by (a) updating the scaling of the edge parameters (from that of [2]) for variations of DT flux and helium density and flux with pumping speed and neutral pressure, (b) removing carbon and introducing seed neon impurity to commence simulation of the later phase of ITER operation, and (c) determining the effect of the impurity seeding on the operating window of ITER following [5,6].

2. Scaling of edge parameters

In previous work ([2] and references therein) the key parameter for determining the edge plasma parameters was found to be,

$$\mu \equiv p_{\mathrm{DT}\#}\, P_{\#}^{-0.87}\, f_{\mathrm{f}}^{-0.8}\, f_{\mathrm{w}}^{-1}\, q_{95\#}^{-0.27}\, f_{\mathrm{nn}}^{-1}\, R_{\#}^{-1.21}. \quad (1)$$

This is proportional to $p_{\mathrm{DT}\#}$, the normalised average divertor neutral pressure at the entrance to the private flux region. Here $R_\#$ represents the normalised divertor radius, $P_\#$ the power entering the SOL normalised by $R_\#^3$, and $q_{95\#}$, the normalised safety factor. The normalisation factors are given in Table 1 of [2], as are the other factors depending on type of fuelling, wall, and neutral model, respectively f_{f}, f_{w} and f_{nn}. (Note that Table 1 of [2] contained an error: the normalisation factor of μ should be 1, and that of $p_{\mathrm{DT}\#}$ should be 8.5).

The edge-based density limit is taken to occur at detachment of the inner divertor ($\mu = 1$) because of increased neutral influx to the core beyond this point. As shown in [2] the DT separatrix density varies as $\mu^{0.43}$, i.e. the density analogue of μ is the ratio of the edge density to that at detachment, $f_{\mathrm{sat\_n}} = \mu^{0.43}$.

Initial results reported in [2] with the nonlinear neutral model indicated that the DT neutral flux was higher (factor 2) and the helium density and flux at the separatrix were lower (factor 0.33) than for the less complete linear neutral model but the scaling had then not yet been determined. We have now varied both pumping speed and throughput (i.e. $p_{\mathrm{DT}\#}$), with results in Fig. 1. Both the original dome F12 and a more recent smaller dome, F47 (see [4]) are shown, the latter with two different pumping speeds. The fit is performed taking into account all of the points in Fig. 1, and the fit values are then given for every one of these points.

The results can be well represented by:

$$\Gamma_{\mathrm{DT}} \equiv 36 f_{\mathrm{f}}^{-4.3}\, S_{\#}^{0.5} f_{\mathrm{w}}^{0.44}\, q_{95\#}^{-0.2} R_{\#}^{1.03} \mu^{0.7}\ [\mathrm{Pa\text{-}m^3\ s^{-1}}], \quad (2)$$

* Corresponding author.
E-mail address: pacher@emt.inrs.ca (H.D. Pacher).
[1] Present address: ITER Organization, Cadarache Centre, F-13108 St. Paul lez Durance, France.

0022-3115/$ - see front matter Crown Copyright © 2009 Published by Elsevier B.V. All rights reserved.
doi:10.1016/j.jnucmat.2009.01.089

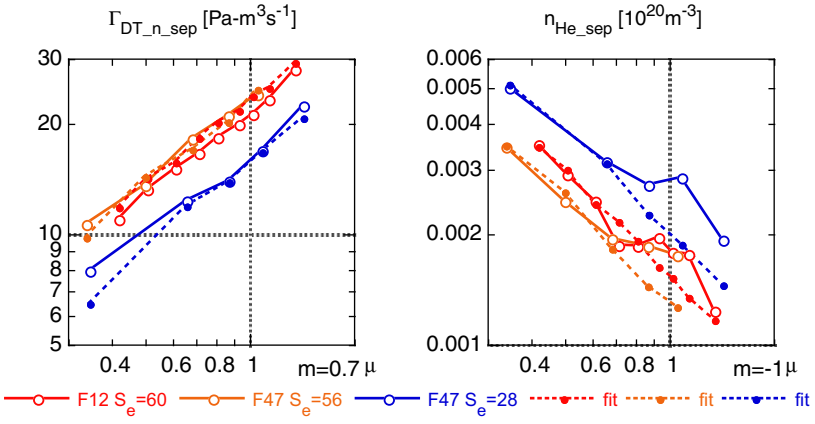

Fig. 1. DT neutral flux (a, left) and helium density (b, right) at the separatrix versus μ (Eq. (1) and text), proportional to DT neutral pressure in the divertor, for two different dome configurations (F12 and F47, see text) and engineering pumping speed S_e in m^3s^{-1}: 60 (F12), 56 (F47) and 28 (F47). 'Fit' are the values from Eqs. (2) and (3) at low-μ.

$$\begin{aligned} &n_{\mathrm{He\_sep}} = k_{\mathrm{n\_He}}\mu^{-1} && \text{for } \mu < 0.65, \\ &k_{\mathrm{n\_He}}\mu^{-1}t < n_{\mathrm{He\_sep}} < k_{n_{\mathrm{He}}}(0.65)^{-1} && \text{for } 0.65 < \mu < 1, \end{aligned} \tag{3}$$

where $k_{\mathrm{n\_He}} = 0.001 f_{\mathrm{He}} f_{\mathrm{f}}^{-4} S_{\#}^{-0.7} \zeta_{\mathrm{ei}}^{-0.1} q_{95\#}^{-0.85} P_{\#}^{0.79} R_{\#}^{0.15}$ [10^{20} m^{-3}].

$$\begin{aligned} &\Gamma_{\mathrm{He\_n\_sep}} = k_{\Gamma\_\mathrm{He}}\mu^{-0.86} && \text{for } \mu < 0.65, \\ &k_{\Gamma\_\mathrm{He}}\mu^{-0.86} < \Gamma_{\mathrm{He\_n\_sep}} < k_{\Gamma\_\mathrm{He}}(0.65)^{-0.86} && \text{for } 0.65 < \mu < 1, \end{aligned} \tag{4}$$

where $k_{\Gamma\_\mathrm{He}} \equiv 0.08 f_{\mathrm{He}} f_{\mathrm{f}}^{-2} S_{\#}^{-0.7} P_{\#}^{0.22} R_{\#}^{-1.46}$ [Pa m^3 s^{-1}].

Here $S_{\#}$ is the engineering pumping speed for D2 molecules at the duct entrance, normalised to 114 m^3 s^{-1} (see discussion in [3], Section 2).

These low-μ fits extrapolated to $\mu = 1$ for dome F12 are close to the preliminary factors of [2] relative to the less complete linear neutral model, i.e. 2.44, 0.37, and 0.3 for DT flux, helium density, and helium flux, respectively. The variation with pumping speed and with μ is stronger for the DT flux and weaker for the helium quantities than for the linear model, and, importantly the helium quantities increase much less rapidly toward lower DT pressure than the previous scaling based on the linear model (exponents 1 and 0.86 rather than 2 and 2). As seen in Fig. 1, the smaller dome F47 results in slightly lower helium levels. For the more complete nonlinear model, the helium quantities depart from the low-μ fits above $\mu > 0.65$, are up to 50% higher at $\mu = 1$, and then decrease again.

3. Effect of neon impurity seeding on the edge and divertor plasma

Impurity seeding is useful to reduce the peak power load on a future carbon-free divertor. We have varied the neon concentrations at the separatrix in the range $0.001 < c_{\mathrm{Ne}} < 0.03$. In order not to vary too many parameters simultaneously, for this study we have used the same particle and energy reflection coefficients at the wall as for carbon, but with zero carbon erosion. Further studies with the parameters appropriate for tungsten will follow. (A variant, several runs with neon, full beryllium walls and self-consistent beryllium sputtering, yielded low Be concentration $c_{\mathrm{Be}} \sim 0.005$ and low Be radiated power 2–4 MW, with other values similar to the carbon-free cases with neon so that this will not be discussed further.)

The resulting radiated power for dome F12 (Fig. 2(a)) varies little with c_{Ne} for $c_{\mathrm{Ne}} > 0.01$, and is slightly below the radiation in the carbon case. However (Fig. 2(b)) the radiation in the inner divertor volume for the Ne cases is 2/3 the value for the C case at $\mu = 1$, down to 1/3 at lower pressures (for the outer divertor volume, the corresponding values are 100% and 80%). This is attributed to the energy-independent chemical erosion for the C case and the low radiation of neon below 10 eV. The plasma at the inner divertor target remains somewhat hotter (Fig. 3(a)) and the power to that target is higher than with C for $\mu < 1$. Detachment is described by the same μ for C and Ne, i.e. no additional factor is required. Whereas for C and for neon at low c_{Ne} the power maximum is on the outer divertor plate, it is on the inner divertor plate for $c_{\mathrm{Ne}} > 0.01$ and $\mu < 1$. For the inner target with neon, the scaling is similar to that for the outer target with carbon, but the numerical value is 30% lower and independent of c_{Ne} in this range. (Since the maximum does not occur on the same divertor plate as for C, differences in flux expansion, divertor plate angle, and divertor length also play a role). Therefore, to a good approximation,

$$q_{\mathrm{pk}}|^{\mathrm{Ne}} = 0.7 q_{\mathrm{pk}}|^{\mathrm{C}}. \tag{5}$$

With the nonlinear neutral model, $q_{\mathrm{pk}}|^{\mathrm{C}}$ is given by the scaling of [2] for dome F47, and 1.2 times this scaling for the older dome F12.

The DT density varies strongly with c_{Ne} at given throughput (i.e. the same μ), Fig. 4(a). As c_{Ne} increases for $c_{\mathrm{Ne}} \geqslant 0.01$, the power available for DT dissociation, ionisation, and excitation decreases and n_{DT} decreases. To a very good approximation (Fig. 4(b)),

$$n_{\mathrm{DT\_sep}}|^{\mathrm{Ne}} + 40 n_{\mathrm{Ne\_sep}}|^{\mathrm{Ne}} = 1.45 n_{\mathrm{DT\_sep}}|^{\mathrm{C}} \mu^{-0.34} \quad \text{for } c_{\mathrm{Ne}} \leqslant 0.01, \tag{6}$$

$n_{\mathrm{DT\_sep}}|^{\mathrm{C}}$ is given by the scaling of [2] for dome F47, $\sim\mu^{0.43}$, and 0.8 times this scaling for the older dome F12.

Neon is ionised to 8.8 at the separatrix, and the total ionisation energy required to attain this state is about 100 times that of DT per atom. Given the profiles of Z, different residence times and different ratios of excitation to ionisation of Ne and DT, the factor 40 in Eq. (6) is broadly consistent with this ratio. The decrease in n_{DT} engenders a strong decrease in n_{e}, albeit somewhat smaller (80% over the range shown) than that of n_{DT}, and this in turn is responsible for the fact that the radiated power is almost invariant with c_{Ne} for $0.01 < c_{\mathrm{Ne}} < 0.03$.

As the neon concentration increases, the helium density and neutral flux at the separatrix progressively decrease by factors of 2.2 and 7.5, respectively, below Eqs. (3) and (4). This is tentatively attributed to lower DT and electron densities in the divertor plasma, leading to lower opacity of this plasma to neutrals and more efficient pumping (the reduction of helium is stronger in the inner divertor), but the details remain to be worked out.

4. Operating diagram

The scaling relations of [2] and the present updated values, including those for neon seeding, from Eqs. (1)–(5), are input

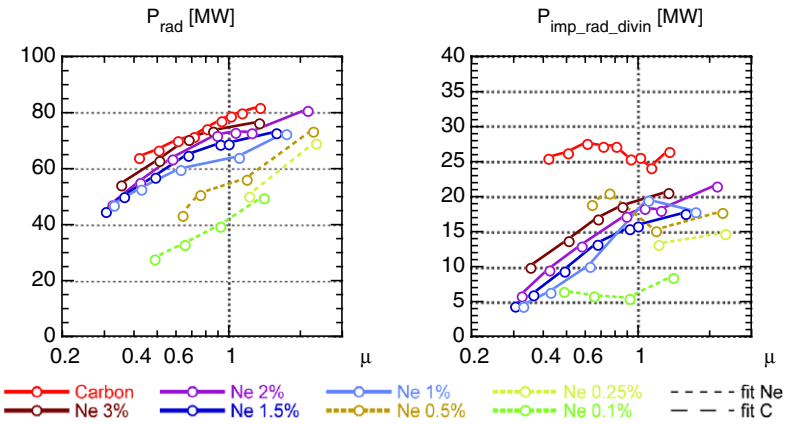

Fig. 2. Radiated power, both total (a, left) and within inner divertor volume (b, right) versus low-μ (Eq. (1)), for carbon and for carbon-free operation with separatrix neon concentrations marked in legend. 'Fit Ne' and 'Fit C' are fits given in the text (used in subsequent figures).

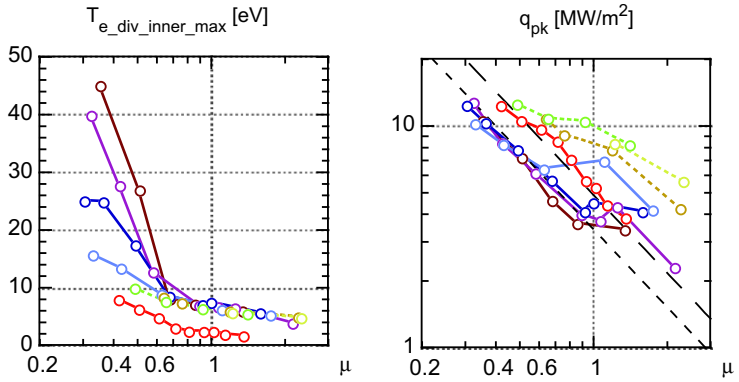

Fig. 3. Maximum electron temperature at the inner divertor plate (a, left) and maximum peak power per unit area on either divertor plate (b, right) versus low-μ (Eq. (1)) for cases and legend of Fig. 2.

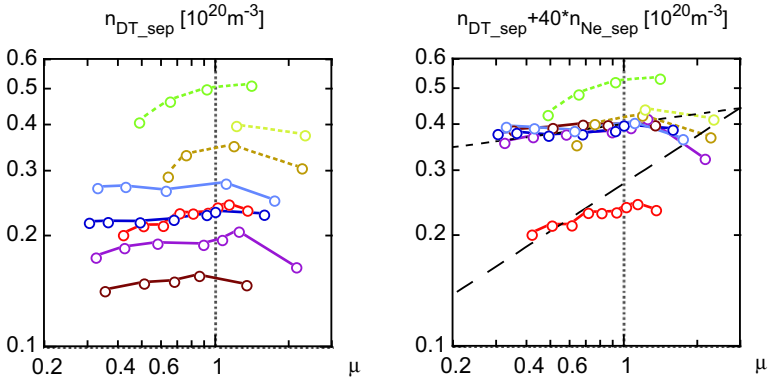

Fig. 4. DT density n_{DT_sep} (a, left) and combined density $n_{DT\_sep} + 40n_{Ne\_sep}$ (b, right), at the separatrix versus low-μ (see Eq. (1), for cases and legend of Fig. 2.

quantities to the core plasma simulations with the integrated model described in preliminary form in [5] and in detail in [6]. Since direct coupling of the core and edge regions is impractical because of the different timescales involved, in this model outer boundary conditions for the core are applied as obtained from SOL/divertor runs, and inner boundary conditions from the core simulations are applied to determine the state of the SOL/divertor at the interface between the core-pedestal (1.5D code ASTRA), and SOL–divertor (2D code B2–EIRENE) regions, thus assuring consistency of operating conditions in both regions (Section 2.2 of [6]). Inputs to the ASTRA simulations from the SOL/divertor scaling include separatrix DT and He densities, separatrix ion and electron temperatures, and separatrix inward neutral DT and He fluxes. Outputs from ASTRA (inputs to the scaling relation) are the power transported across the separatrix by electrons and by ions, the fusion power, and the DT flux into the SOL. (The He ion flux is the sum of production by fusion and neutral influx). The control parameters for the core simulation are the core fuelling flux Γ_{DT_core}, the gas puff flux into the vessel $\Gamma_{DT\_n\_puff}$, and the additional heating power P_{aux}. The separatrix density and neutral influx are also transmitted to Astra for any impurities included in the 2D modelling. For the simulations presented here, this is either the intrinsic carbon

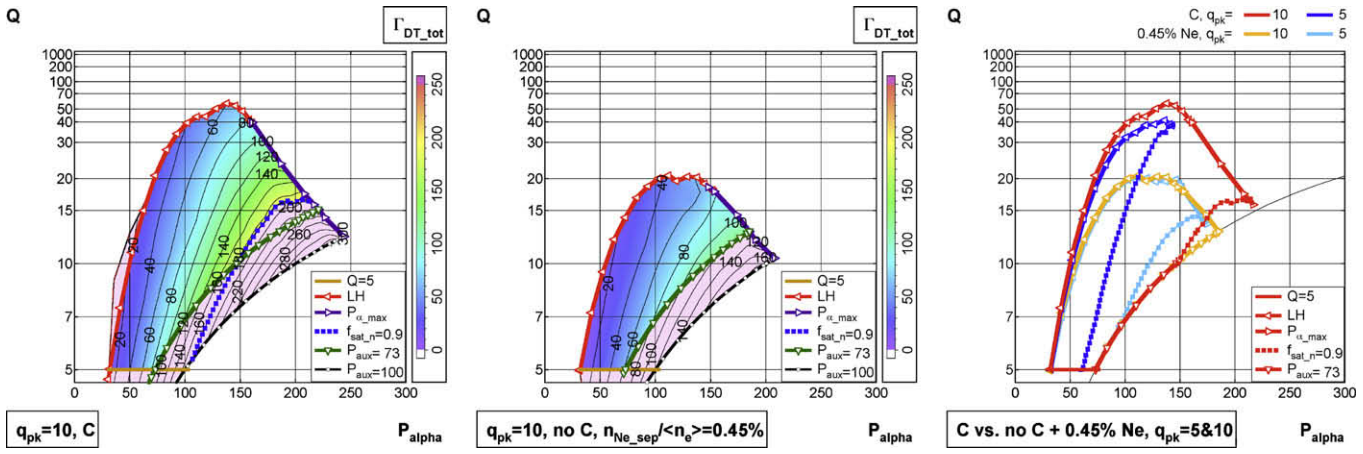

Fig. 5. ITER operating diagram in the plane Q versus alpha particle power P_{alpha} with limiting curves (see text) for $Q = 5$, LH transition, P_{alpha_max}, edge density limit $f_{sat\_n} = \mu^{0.43} = 0.9$, and $P_{aux} = 73$MW, with contours of total DT throughput Γ_{DT_tot} for peak power $q_{pk} = 10$ with carbon walls (left) and carbon-free walls with neon density $n_{Ne\_sep}/\langle n_e\rangle = 0.45\%$ (middle). Operating diagrams with $q_{pk} = 10$ and 5, carbon and carbon-free walls are superposed (right). Area outside limits indicated white or pink in left and middle.

impurity self-consistently produced by plasma interaction with the divertor plates, or the seeded impurity neon. For the latter case, the separatrix neon density constitutes an independent input parameter.

The model of [5,6] calculates the edge pedestal width and height and has been shown [6] consistent with experimental scalings of pressure at the top of the pedestal. Following [5,6], we determine the operating window characterising ITER performance in the space Q -P_{alpha}. The window is determined by five limits: (1) $Q = 5$, (2) the LH back transition, taken equal to the forward transition to provide a margin, (3) P_{alpha_max}, the low-temperature limit beyond which higher density no longer yields higher fusion power, (4) the edge density limit determined from the edge scaling at detachment with a margin 0.9, $f_{sat\_m} = \mu^{0.43} = 0.9$, replacing the Greenwald limit, and (5) the available external power P_{aux}. (The beta limit is not attained here [6]).

Each operating window corresponds to a constant q_{pk}, which is adjusted by gas puffing and/or neon seeding. Gas puffing in ITER yields little core fuelling, $\sim$20 Pa m^3 s^{-1} (Fig. 1) because of the SOL opacity to neutrals, so that core fuelling must be provided differently (e.g. shallow pellet injection $r/a = 0.85$). Both with C and neon, the helium concentration is low for these conditions and has little effect on the operating window.

The operating window is shown in Fig. 5 for carbon cases and for carbon-free cases with a ratio $n_{Ne\_sep}/\langle n_e\rangle = 0.45\%$, which corresponds to $n_{Ne\_sep}/n_{e\_sep} = 1$—1.5% across the window i.e. the scaling of Section 3 for q_{pk} and n_{DT} is valid. Despite the lower q_{pk} with neon (Eq. (5)) the operating window is reduced both in Q and P_{α} (Fig. 5) at $q_{pk} = 10$, where the edge density limit does not play a strong role. However, with neon the core fuelling required for the same P_{alpha} is somewhat larger, but less gas puffing is needed so that the total throughput is smaller by a factor 2 (Fig. 5). Another method of reducing throughput, reducing the pumping speed, was found to have little effect on the operating window down to 0.5 of the nominal pumping speed but beyond that the edge density limit acts and reduces the attainable P_{alpha} [6].

When a more stringent condition, $q_{pk} = 5$, is specified and very strong gas puffing would be required, the edge density limit strongly constricts the operating window at high P_{alpha}, and neon seeding then increases the operating window in P_{alpha} (but not in Q since neon core radiation reduces the SOL power and the LH transition margin).

5. Conclusions

Previously obtained scaling laws from edge modelling have been updated, and the effect of neon seeding has been determined. DT neutral influx to the core is higher than with less complete models but still remains small, whereas the helium scaling toward lower DT pressures is more benign than previous scalings. With neon seeding in carbon-free cases, the radiated power is similar to that with carbon but the peak power load shifts to the inner divertor plate and is 30% lower, and both helium density and neutral flux are again reduced. The major effect is on the deuterium density, which decreases strongly as neon concentration increases because less power is available for DT ionisation. These relations are used as inputs to core modelling to determine the operating window. Impurity seeding leads to an increase in the operating window only when a lower, more stringent peak power condition is specified and excessive gas puffing would be required to achieve it. For moderately high peak power levels, neon seeding reduces the operating window; it has, however, the advantage of lowering the throughput required for a given peak power load and, although this has no effect on the operating window for these parameters, reducing the helium density and influx. In future work, the transition to carbon-free divertor operation with low seeding will be further explored and the reflection coefficients and erosion appropriate for tungsten will be introduced.

References

[1] A.S. Kukushkin, H.D. Pacher, V. Kotov, et al., Nucl. Fus. 45 (2005) 608.
[2] H.D. Pacher, A.S. Kukushkin, G.W. Pacher, et al., J. Nucl. Mater. 363–365 (2007) 400.
[3] A.S. Kukushkin, H.D. Pacher, V. Kotov, et al., J. Nucl. Mater. 363–365 (2007) 308.
[4] A.S. Kukushkin, H.D. Pacher, V. Kotov, et al., in: Proceedings of the 34th EPS Conference on Plasma Physics, European Physical Society, Warsaw, 2007.
[5] G.W. Pacher, H.D. Pacher, A.S. Kukushkin, et al., in: Proceedings of the 34th EPS Conference on Plasma Physics, European Physical Society, Warsaw, 2007.
[6] G.W. Pacher, H.D. Pacher, G. Janeschitz, A.S. Kukushkin, Nucl. Fusion 48 (2008) 105003 (26 pp).